

Wave Packet Simulations of Antiproton Scattering on Molecular Hydrogen

Henrik Stegeby,¹ Markus Kowalewski,² Konrad Piszczatowski,¹ and Hans O. Karlsson^{1, a)}

¹⁾*Department of Chemistry - Ångström, Uppsala University Box 518, 75120 Uppsala, Sweden*

²⁾*Department of Information Technology, Uppsala University Box 337, 75105 Uppsala, Sweden^{b)}*

(Dated: 11 August 2024)

The problem of antiproton scattering on the molecular hydrogen is investigated by means of wave packet dynamics. The electronic potential energy surfaces of the antiproton H_2 system are presented within this work. Excitation and dissociation probabilities of the molecular hydrogen for collision energies in the ultra low energy regime below 10 eV are computed.

PACS numbers: 36.10-k, 34.50.Ez

Keywords: Potential energy surface; low energy scattering; matter-antimatter interactions; antiproton scattering; molecular hydrogen scattering

I. INTRODUCTION

The antimatter-matter asymmetry is an active area of physics addressing fundamental questions concerning the evolution of the universe, the validity of the CPT symmetry and gravitational differences between matter and antimatter^{1,2}.

Even though our universe seems to be solely composed of regular matter it is possible to create and study antimatter in the laboratory^{3,4}. The recent advances in the field of antimatter include the production and trapping of antihydrogen⁵ as well as cooling to a stable electronic state⁶. Antihydrogen is one of the simplest examples of an atomic system composed of antimatter. However, to increase the understanding of antimatter systems the interaction between matter and antimatter is of special interest. Mixed matter-antimatter many-body systems provide a field of study, which exceeds the pure annihilation effects and allows for comparison with the dynamics of ordinary molecular systems. Examples of such many body systems includes, e.g., antihydrogen-hydrogen⁷, antiprotonic helium^{8,9} and various antiproton - gas collisions investigated by the ASACUSA collaboration in the antiproton collisional kinetic energy regime of 2-11 keV¹⁰.

In this work we have investigated the collision an antiproton (\bar{p}) with molecular hydrogen as a model system for more complex antiparticle - molecular interactions. The $H_2\text{-}\bar{p}$ system is interesting from a practical point of view as residual H_2 gas exists in most high energy colliders, and antiprotons are created in various experiments, resulting in scattering of antiprotons on H_2 molecules⁹. Previous work on this system focused on the high-energy¹¹ and the low-energy collision region investigating antiproton and proton cross sections for ionization

and excitation of hydrogen molecules as well as energy spectra of the ionized electrons^{10,12-14}.

In previous work the influence of collisions in the energy regime above 100 eV was investigated which mainly leads to ionized reaction products¹⁵. However, the ultra low energy regime below 10 eV¹⁶ opens up a new regime of matter-antimatter chemistry, since this energy is comparable to the chemical bond energy. In this region the molecular hydrogen is vibrationally excited, but remains in its electronic ground state. The antiproton behaves like another nucleus in the molecular system, whereas its negative charge produces an interaction potential, which is on the order of magnitude of an electronic state in an atom.

In this paper we have computed potential energy surfaces (PES) for the lowest electronic states of the $H_2\text{-}\bar{p}$ system and performed wave packet simulations of the collision on the electronic ground state. The wave packet simulation provide information about probability distributions of the vibrational states of the H_2 molecule after the collision, as well as the dissociation probability. The paper is organized as follows: In section II the quantum dynamical model is introduced. In section III the potential energy surfaces (PES) of the $H_2\text{-}\bar{p}$ system and the results of the wave packet calculations are presented followed by a discussion in section IV.

II. QUANTUM DYNAMICS MODEL

We have considered a T-shaped configuration of the $H_2\text{-}\bar{p}$ system corresponding to a zero impact parameter, as illustrated in Fig. 1, which is expected to have a maximum interaction between the antiproton and the vibrational degree of freedom of the molecular hydrogen. Jacobi coordinates are used to describe the inter-atomic distances between the H-atoms (R_{HH}) and the antiproton distance to the center of mass of H_2 ($R_{\bar{p}}$). The angle of the H-H bond axis and $R_{\bar{p}}$ is fixed to be 90 degrees. This choice of coordinates focuses specifically on the vibrational and dissociation dynamics of H_2 in collision

^{a)}Electronic mail: hans.karlsson@kemi.uu.se

^{b)}Electronic mail: mkowalew@uci.edu; Now at: Chemistry Department, University of California, Irvine, California 92697-2025, United States

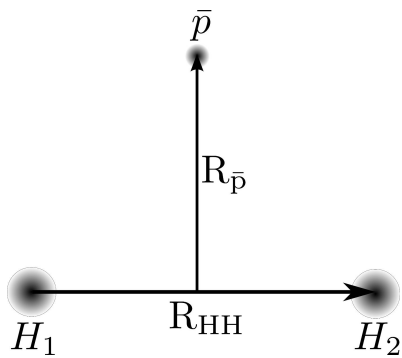


FIG. 1. Jacobi coordinates for the $H_2 - \bar{p}$ system in a T-shaped configuration. The internuclear separation between the hydrogen atoms H_1 and H_2 are varied along the R_{HH} axis and the distance from the barycenter of the two hydrogen atoms to the antiproton is the $R_{\bar{p}}$ axis.

event with \bar{p} . Other reaction pathways like the protonium formation¹⁶ are neglected in this model.

To simulate the collision between the hydrogen molecule and the antiproton we solve the time-dependent Schrödinger equation for the nuclei

$$i\hbar \frac{\partial}{\partial t} \Psi(R_{HH}, R_{\bar{p}}, t) = \hat{H} \Psi(R_{HH}, R_{\bar{p}}, t), \quad (1)$$

numerically. Atomic units are used (i.e. $\hbar = m_e = e = 4\pi\epsilon_0 = 1$) in what follows. The Hamiltonian in Jacobi coordinates reads:

$$\hat{H} = \hat{T}_{R_{\bar{p}}} + \hat{T}_{R_{HH}} + \hat{V}(R_{HH}, R_{\bar{p}}) = -\frac{1}{2\mu_{HH}} \frac{\partial^2}{\partial R_{HH}^2} - \frac{1}{2\mu_{\bar{p}}} \frac{\partial^2}{\partial R_{\bar{p}}^2} + \hat{V}(R_{HH}, R_{\bar{p}}), \quad (2)$$

where R_{HH} , and $R_{\bar{p}}$ are the Jacobi coordinates as defined in Fig. 1. The reduced masses and $\mu_{\bar{p}}$ and μ_{HH} are given by

$$\mu_{HH} = \frac{m_p}{2} \quad (3)$$

$$\mu_{\bar{p}} = \frac{2m_p^2}{(m_p + 2m_p)} = \frac{2}{3}m_p, \quad (4)$$

where m_p is the rest mass of the proton. The choice of the Jacobi coordinates ensures that the system is in the center of mass frame. The molecular potential energy surface (PES) \hat{V} represents the adiabatic electronic ground state potential of the system and is obtained by solving the electronic Schrödinger equation under the assumption that the Born-Oppenheimer approximation is valid. The collision of the molecular hydrogen with the antiproton in the given coordinate system R_{HH} , $R_{\bar{p}}$ is simulated by solving eq. 1 numerically with a Chebyshev time propagation scheme¹⁷. A perfectly matched layer (PML)¹⁸ at the edges of the numerical grid has been used to absorb the wavefunction and to avoid spurious reflections.

The initial condition is chosen to meet the given physical conditions of an antiproton approaching a hydrogen molecule. The initial wave function can be written as a product state of the H_2 vibrational ground state wave function ϕ_0 and a Gaussian wave packet representing the antiproton:

$$\Psi(R_{HH}, R_{\bar{p}}, t = 0) = \sqrt{\frac{2}{\sigma\sqrt{2\pi}}} e^{ikR_{\bar{p}} - (R_{\bar{p}} - R_0)^2 / 2\sigma^2} \phi_0(R_{HH}). \quad (5)$$

The collision energy $\rho_0 = p^2 / 2\mu_{\bar{p}}$ enters eq. 5 through the momentum $p = \hbar k$. The width σ of the wave packet is assumed to be 0.3 Å, which corresponds to a width of 35 meV in kinetic energy. In the limit of $R_0 \rightarrow \infty$ i.e. of separated reactants the PES becomes flat and the Schrödinger equation becomes separable in the molecular coordinates justifying the choice of the wave-packet, eq. 5. A value of $R_0 = 10$ Å is chosen as a good approximation on a finite surface used in the numerical model.

By describing the system with the non-relativistic Schrödinger equation, the particle anti-particle annihilation of the proton and the antiproton is neglected. However, a direct p- \bar{p} collision has a low probability, specially for the given setting (impact parameter of zero). This is justified by the wave packet simulations which show that the probability density of the wave function is low at the positions representing a direct p- \bar{p} contact. A comparison of the simulation time scale for a single collision event with experimentally determined annihilation time constants¹⁵ shows that the annihilation probability is indeed low and annihilation effects are expected to be small and to have no significant influence here.

III. RESULTS

A. Potential energy surfaces

The electronic ground state and the first five excited states potential energy surfaces have been calculated with the full configuration interaction (FCI) method using MOLCAS program package¹⁹. The Atomic Natural Orbital basis set of valence triple zeta accuracy with polarization functions (ANO-L-VTZP) basis set¹⁹ is used to describe the two electrons. The influence of the antiproton on the electronic states of the H_2 molecule is simulated by adding a negative point charge to the geometry definition. A comparison between the ground state and the first few excited electronic state potential energy surfaces (PES) is presented in one-dimensional slices at different antiproton distances in Fig. 2. In Fig. 2 one can see that the electronic ground state is well separated from the excited state surfaces and no avoided crossings or conical intersections between the ground state and an excited state occurs. However, curve crossings can be observed between the $1^1\Pi_g$ and the $2^1\Pi_g$ state at $R_{HH} \approx 1.6$ Å

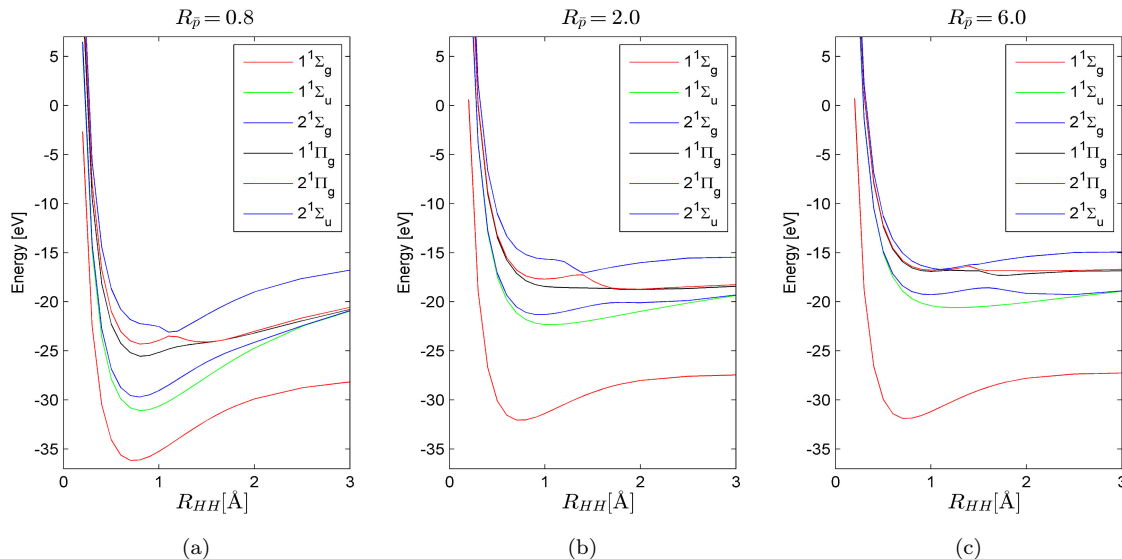


FIG. 2. Slices through the PES for different values of $R_{\bar{p}}$. (a) 0.8 Å, (b) 2.0 Å, and (c) 6.0 Å. The ground state ($1^1\Sigma_g$) and the first - to fifth excited states (H_2 state symmetries $1^1\Sigma_u$, $2^1\Sigma_g$, $1^1\Pi_g$, $2^1\Pi_g$ and $2^1\Sigma_u$) energy are varied along the internuclear separation between the hydrogen atoms R_{HH} . The labels of the electronic states refer to the electronic states of unperturbed H_2 in the $D_{\infty h}$ point group. A potential energy of 0 eV refers to the limit of separated particles.

and $2^1\Pi_g$ and the $2^1\Sigma_g$ state at $R_{HH} \approx 1.2$ Å. Note that for the hydrogen molecule only avoided crossings can occur, whereas the triatomic $H_2-\bar{p}$ system can have conical intersections^{20,21} between states of the same symmetry. As the antiproton approaches the H_2 molecule the PES energy and the difference between the vertical excitation energy and the groundstate energy decreases, while the $1^1\Pi_g$, $2^1\Pi_g$ and $2^1\Sigma_g$ states increase their separation in energy. For the $2^1\Sigma_g$ and $1^1\Pi_g$ excited state crossings have been observed. The groundstate energy curve becomes identical to the ground state curve for unperturbed H_2 as $R_{\bar{p}} \rightarrow \infty$. The dissociative limit of the H_2 groundstate approaches -27.21 eV, which corresponds to the sum of two H atoms in their groundstate, as $R_{HH} \rightarrow \infty$.

A two-dimensional plot of the electronic ground state PES in the T-shaped configuration, is shown in Fig. 3. A deep potential well is found where the antiproton passes through the axis of the molecular hydrogen caused by an attractive Coulomb interaction between the protons and the antiproton. The theoretical value in the origin of the coordinate system $\{R_{HH}, R_{\bar{p}}\}$ can be directly derived from the Coulomb interactions V_C by taking the limit $\{R_{HH}, R_{\bar{p}}\} \rightarrow 0^+$ for the interaction potential:

$$\begin{aligned} \lim_{\{R_{HH}, R_{\bar{p}}\} \rightarrow 0^+} V_C &= \lim_{\{r_{1\bar{p}}, r_{2\bar{p}}, r_{12}\} \rightarrow 0^+} \frac{e_p e_{\bar{p}}}{r_{1\bar{p}}} + \frac{e_p e_{\bar{p}}}{r_{2\bar{p}}} + \frac{e_p^2}{r_{12}} \\ &= \lim_{\{R_{HH}, R_{\bar{p}}\} \rightarrow 0^+} \frac{1}{R_{HH}} - \frac{2}{\sqrt{R_{\bar{p}}^2 + (R_{HH}/2)^2}} \end{aligned} \quad (6)$$

where $r_{1\bar{p}}$, $r_{2\bar{p}}$ and r_{12} are the distances between proton

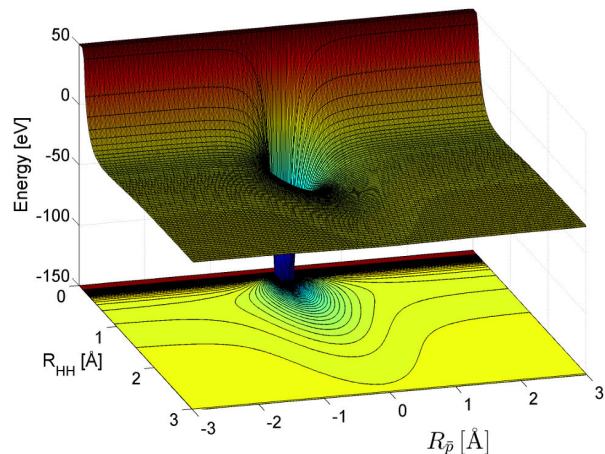


FIG. 3. PES for the $H_2-\bar{p}$ systems ground state, calculated in dependence of the H_2 separation and the antiproton distance. For clarity the potential is truncated above +50 eV. Note that the potential converges to $-\infty$ at (0,0).

1 and the antiproton, proton 2 and the antiproton, and the distance between proton 1 and 2 respectively. Here $e_p \equiv +1$ and $e_{\bar{p}} = -1$ are the charge of the proton and the antiproton respectively. From eq. 6 it becomes clear that the limit diverges to minus infinity. This is indicated in Fig. 3 showing a potential hole diverging to minus $-\infty$.

B. Quantum Dynamics Simulations

The H_2 antiproton collision is simulated by solving eq. 1 numerically using the Chebyshev time propagation scheme¹⁷, combined with the Fourier method²², for different collision energies. The initial conditions are constructed from eq. 5 and cover collisions with an incoming energy between 0.01 and 10 eV. The PES which enters through the Hamiltonian (eq. 2) is the $1^1\Sigma_1$ electronic ground state as it is shown in Fig. 3. We assume that the electronic ground state of the $\text{H}_2\text{-}\bar{p}$ system is sufficient to describe the collision in the energy regime considered. This is justified by the absence of curve crossings between the ground state and the excited states.

The time evolution of a wave packet with an initial kinetic energy of 3 eV is shown in Fig. 4 for 3 different times. As the wave packet approaches the deep potential well the strong attraction of the Coulomb force becomes visible (Fig. 4b)). When the antiproton transverses the potential singularity, the wave function is either reflected, transmitted, or deflected towards the H_2 dissociation. As the potential is a conservative potential in this model the wave packet can not be trapped in the location around the potential singularity. Eventually it will be scattered into separate fragments. The quantitative results of the inelastic scattering event will be presented in the following sections.

1. H_2 vibrational excitation

The vibrational excitation after the collision event is analyzed separately for the reflected and the transmitted part of the wave function. In the asymptotic limit of a large $|R_{\bar{p}}|$ the Schrödinger equation for the Hamiltonian (eq. 2) becomes separable and the vibrational excitation can be expressed in terms of vibrational eigenfunctions $\phi_\nu(R_{HH})$ of H_2 . The probability of finding the system in a vibrational eigenstate ϕ_ν at a certain time t is given by the projection against the total nuclear wave function $\Psi(R_{HH}, R_{\bar{p}^0}, t)$:

$$|c_\nu(t)|^2 = \int |\phi_\nu(R_{HH})\Psi(R_{HH}, R_{\bar{p}^0}, t)|^2 dR_{HH}. \quad (7)$$

The distance from the H_2 center is chosen to be $R_{\bar{p}^0} = 10$ Å, which is far enough from the interaction region such that the separability assumption is sufficiently fulfilled. The total probability P_ν is then obtained by integrating eq. 7 over time²³:

$$P_\nu = \frac{1}{N^\tau} \int_0^\tau |c_\nu(t)|^2 dt. \quad (8)$$

The time end point τ (500 fs) is chosen such that less than 1% of the wave packet remains after absorption at the PML. A time step 242 as has been chosen and is sufficiently short to allow for an accurate numerical integration over time.

The antiproton is scattered in all directions and integral bounds have to set such that the reflected part of the wave function Ψ_R and the transmitted part of the wave function Ψ_T is captured. The sum over the coefficients corresponding to the these probability distributions is the normalization coefficient N^τ we use, i.e.

$$N^\tau = \sum_\nu \left(\int_{t=0}^\tau |c_\nu^R(t)|^2 dt + \int_{t=0}^\tau |c_\nu^T(t)|^2 dt \right). \quad (9)$$

The normalization N^τ is chosen such that the sum of the probabilities for the reflected and transmitted part is unity.

The total probability for the elastic scattering $P^E(\nu = 0)$ is given by

$$P_{\nu=0}^E = \frac{\int_{t=0}^\tau |c_0^R(t)|^2 dt + \int_{t=0}^\tau |c_0^T(t)|^2 dt}{N^\tau}, \quad (10)$$

which, together with the dissociation probability P_{diss} described in section III B 2 gives the resulting inelastic scattering probability.

The vibrational distributions for the transmitted and reflected part are shown in Fig. 5. Until 0.1 eV elastic scattering dominates the process and H_2 remains in its vibrational ground state. At 0.28 eV the reflected part begins to slightly broaden its vibrational distribution while the transmitted part still remains in $\nu = 0$. This is the main difference between the reflected and the transmitted vibrational distributions, which otherwise are very similar. As the kinetic energy is increased further, ν displays a broad distribution of the vibrational states. For comparison the mean vibrational quantum numbers

$$\langle \nu \rangle = \sum_{\nu=0}^{14} \nu P_\nu \quad (11)$$

of the H_2 vibrations after the collision are shown in Fig. 6. Due to the small difference between the reflected and transmitted parts only the sum of both is shown. The mean vibrational quantum number increases linearly until the H_2 dissociation energy of 4.52 eV and peaks around 7 eV with a maximum around $\langle \nu \rangle = 10$. The mean vibrational quantum number can be regarded as a good measure until about 6 eV where the dissociation probability reaches a threshold and increases.

2. H_2 Dissociation

The dissociation probability of H_2 is analyzed by using the probability flux derived from the continuity equation²⁴:

$$\frac{\partial \Psi^* \Psi}{\partial t} + \nabla \cdot \vec{j} = 0, \quad (12)$$

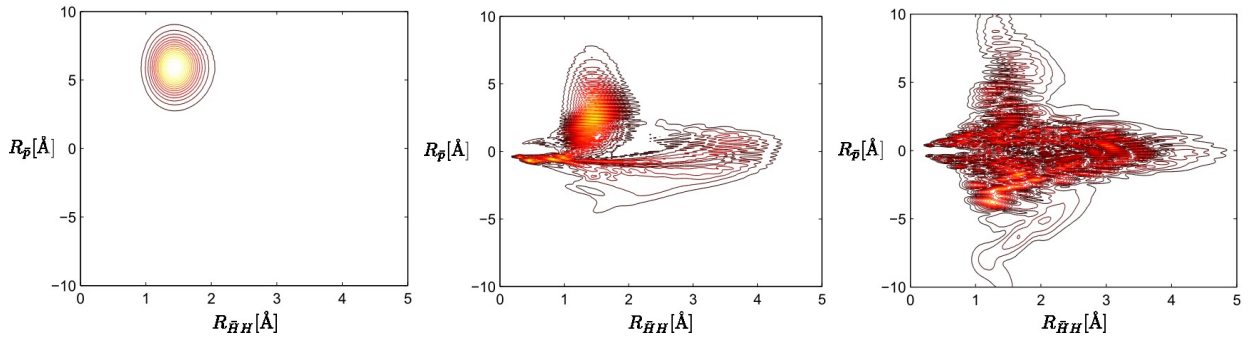
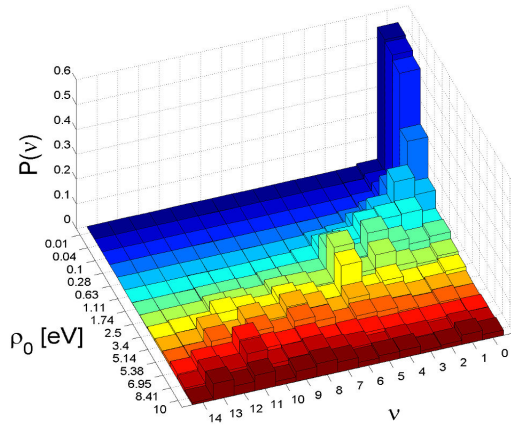
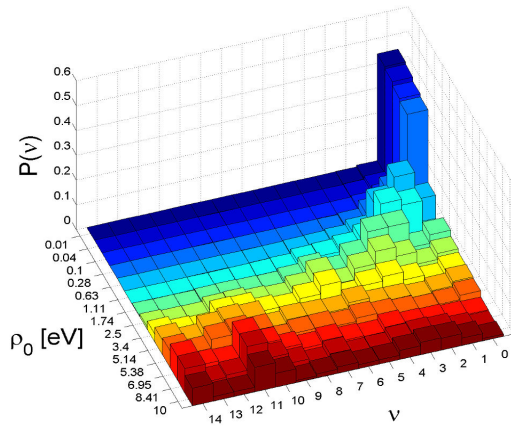


FIG. 4. Time evolution of the antiproton wave packet with a kinetic energy of $\rho_0 = 3\text{eV}$ at times $t = 60\text{ fs}$, $t = 110\text{ fs}$ and $t = 160\text{ fs}$ (from left to right).



(a)



(b)

FIG. 5. The probability distribution for the reflected (a) and the transmitted (b) wavefunction for the H_2 molecule to end up in vibrational excitation state $\nu=0$ to 14 versus initial antiproton kinetic energy ρ_0 . The probabilities of both diagrams sum up to one for a specific energy value.

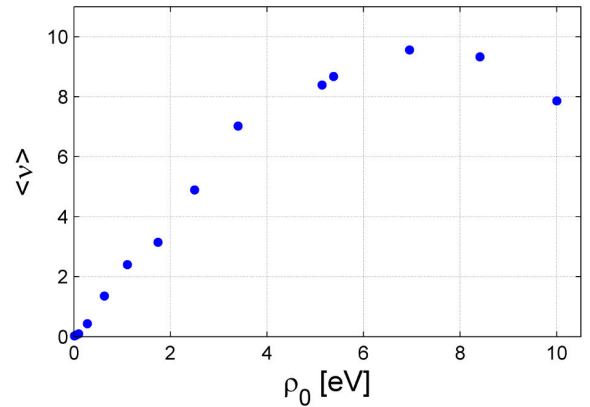


FIG. 6. The mean vibrational quantum number $\langle \nu \rangle$ distribution versus initial antiproton kinetic energy ρ_0 for the sum of the reflected and the transmitted wavefunction.

where \vec{j} is the probability flux. Eventually, the probability flux $F(t)$ reads:

$$F(t) = -\frac{2}{\hbar} \int_V \Im \left(\Psi(R_{HH}, R_{\bar{p}}, t)^* \hat{T} \Psi(R_{HH}, R_{\bar{p}}, t) \right) dV, \quad (13)$$

where \Im denotes the imaginary part, and V is the volume corresponding to a bound H_2 in the coordinate system R_{HH} , $R_{\bar{p}}$. The operator \hat{T} is the kinetic operator from the Hamiltonian (eq. 2). By using a step function $\Theta(R_{HH} - R_{HH,0})$ which drops to zero at $R_{HH} = 15\text{ \AA}$, the probability flux describing the dissociation of H_2 is obtained:

$$F_{diss}(t) = -\frac{2}{\hbar} \int_{-\infty}^{\infty} \Theta(R_{HH} - R_{HH,0}) \times \Im \left(\Psi(R_{HH}, R_{\bar{p}}, t)^* \hat{T} \Psi(R_{HH}, R_{\bar{p}}, t) \right) d\mathbf{R}. \quad (14)$$

The integration over time yields the dissociation probability:

$$P_{diss} = \int_0^T F_{diss}(t) dt \quad (15)$$

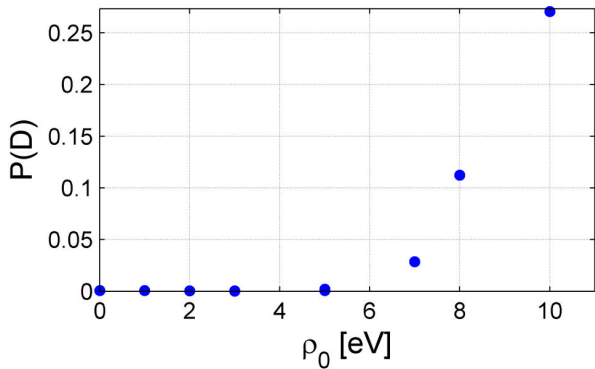


FIG. 7. Dissociation probability $P(D)$ of the H_2 molecule versus initial antiproton kinetic energy ρ_0 , displaying a rapidly growing behavior after 6 eV.

The dissociation probability is shown in Fig. 7. It is close to zero until it reaches a dissociation threshold at 6 eV. Between 7 and 10 eV the dissociation probability increase linearly to 25%. Note that the dissociation energy of H_2 is 4.52 eV.

IV. DISCUSSION

The ground state of the $H_2-\bar{p}$ system is separated by more than 5 eV from the first excited state, which can be seen from Fig. 2, and thus the effect of non-adiabatic couplings can be neglected if the H_2 is initially in its electronic ground state. We notice, however, that the excited states $2^1\Pi_g$ and $2^1\Sigma_u$ of the coupled system show clearly a region of curve crossing (Fig. 2(b)), which needs to be taken in consideration for higher collision energies. In a three body system an avoided crossing can become a conical intersection (CI)²⁰ with a truly degenerate point. The third degree of freedom necessary to form a CI originates from an anti matter particle with a negative charge instead of an ordinary nucleus, making it a special case. This can also be viewed as a more general case of CIs. Other examples for introducing CIs through a non-standard nuclear degree of freedom are light induced CIs²⁵.

The ground state potential in two dimensions (Fig. 3) demonstrates the unique features of the interaction with a negative charge and the hydrogen molecule. The PES is characterized by its deep Coulomb hole diverging to minus infinity. The form of the potential suggests that a bound vibrational ground state could exist. However, this ground state – representing a captured antiproton – could be subject to strong annihilation effects and short lived. In contrast to a tri-atomic molecule the $H_2-\bar{p}$ ground state is expected to be several keV deep²⁶ due to the mass of the antiproton (compared to an electron). Its determination and investigation however is beyond the scope of this paper.

The analysis of the vibrational distribution of H_2 (Fig. 5) shows a clear threshold in collision energy below which the reaction products are mainly in the vibrational ground state. This threshold value is between 0.28 and 0.63 eV and is consistent with the first vibrational excitation of H_2 at 0.55 eV²⁷. However, the distribution has a slight asymmetry between the reflected and transmitted part at 0.28 eV. This indicates that the slightly longer interaction time for the reflected part allows coupling of some of the antiproton’s kinetic energy into the H_2 mode. For collision energies beyond 3.4 eV the vibrational distribution becomes more spread out, which can be explained by the anharmonicity of the H_2 : at higher collision energy more vibrational levels become accessible. Here the mean vibrational quantum number $\langle\nu\rangle$ (Fig. 6) provides a more clear picture. The increase in $\langle\nu\rangle$ is close to a linear behavior for collision energies below 4 eV. A comparison with the energy of $\nu = 7$ (2.9 eV) and the collision energy leads to the conclusion that approximately 90% of the antiproton’s kinetic energy is converted into vibrational energy.

At a collision energy of ≈ 6 eV the H_2 begins to dissociate (Fig. 7). However at least 8 eV is necessary to dissociate about 10% of the H_2 . Compared with the dissociation energy of 4.52 eV of H_2 this is a remarkable excess of energy which is needed to induce the H_2 dissociation. This indicates that the coupling between the antiproton mode and the H_2 mode becomes more inefficient with increasing collision energy. Such effects have been observed in other reactive scattering systems in the form of a dynamical barrier²⁸. A simple explanation for this phenomena could be provided by the fact, that the interaction time between the H_2 and the antiproton becomes shorter at higher velocities and reduces the effective time to transfer energy between the modes.

V. CONCLUSIONS

To describe the dynamics of an antiproton colliding with a hydrogen molecule the electronic PES of the ground state as well as for the five lowest excited states were first computed. The quantum chemical calculations show that it is enough to include the ground state PES to describe the dynamics in the ultra low energy regime considered here. For higher collision energies it might be necessary to include non-adiabatic couplings, as indicated by the curve crossings between the excited states. The possibilities of finding conical intersection instead of avoided crossings, compared to bare H_2 , is an exciting example of non-conventional conical intersections. A thorough analysis will be conducted in a future paper. The results of the wave packet dynamics give insight into the energy redistribution during the collision. For energies below the dissociation threshold the scattering event leaves a clear signature in the vibrational distribution of the H_2 system. The vibrational excitations are in accordance with the H_2 vibrational states. The system has a

clear threshold with respect to dissociation. The theoretical calculations show that this threshold is ≈ 1.5 eV above the dissociation limit of H_2 .

ACKNOWLEDGMENTS

M.K. acknowledges support through the Centre of Interdisciplinary Mathematics (CIM), Uppsala University. H.S. acknowledges support from Roland Lindh, and want to thank Alejandro Saenz and Armin Lühr for helpful discussions concerning the $H_2 - \bar{p}$ scattering problem, as well as Mickael G. Delcey for help regarding the MOLCAS program package. The computations were performed on resources provided by SNIC through Uppsala Multidisciplinary center for Advanced Computational Science (UPPMAX) under Project snic2013/1-267

- ¹The ALPHA collaboration, *Nature Comm.* **4**, 1785 (2013).
- ²M. Villata, *Europhys. Lett.* **94**, 20001 (2011).
- ³G. Baur et al., *Phys. Lett. B* **368**, 251 (1996).
- ⁴D. G. Christian et al., *Am. Phys. Soc.* **42**, 951 (1997).
- ⁵N. Madsen, *Philos. T. R. Soc. A: Mathematical, Physical and Engineering Sciences* **368**, 3671 (2010).
- ⁶The ALPHA collaboration, *Nature Phys.* **7**, 558 (2011).
- ⁷H. Stegeby, K. Piszczatowski, H. O. Karlsson, R. Lindh, and P. Froelich, *Cent. Eur. J. Phys.* **10**, 1038 (2012).
- ⁸The ASACUSA collaboration, *Phys. Lett. B* **700**, 1 (2011).
- ⁹A. Hiroyuki, M. Torii, Shibata, H. Imao, P. Crivelli, Y. Nagata, D. Barna, M. Hori, Y. Kanai, A. Mohri, L. V. Varentsov, and Y. Yamazaki, *J. Phys. Conf. Series* **80**, 012022 (2007).
- ¹⁰The ASACUSA collaboration, *Phys. Rev. Lett.* **105**, 213201 (2010).
- ¹¹M. S. Pindzola, L. Teck-Ghee, and J. Colgan, *J. Phys. B: At. Mol. Opt. Phys.* **43**, 235201 (2010).
- ¹²A. Luehr and A. Saenz, *Phys. Rev. A* **78**, 032708 (2008).
- ¹³A. Luehr and A. Saenz, *Hyperfine Interactions* **194**, 59 (2009).
- ¹⁴D. V. F. I. B. Abdurakhmanov, A. S. Kadyrov and I. Bray, *Phys. Rev. Lett.* **111**, 173201 (2013).
- ¹⁵M. Agnello, G. Belli, G. Bendiscioli, A. Bertin, E. Botta, T. Bressani, M. Bruschi, M. P. Bussa, L. Busso, D. Calvo, B. Cereda, P. G. Cerello, C. Cicalò, M. Corradini, S. Costa, S. De Castro, A. Donzella, A. Feliciello, L. Ferrero, A. Filippi, V. Filippini, A. Fontana, D. Galli, R. Garfagnini, B. Giacobbe, P. Gianotti, A. Grasso, C. Guaraldo, F. Iazzi, A. Lanaro, E. Lodi Rizzini, V. Lucherini, S. Marcello, U. Marconi, A. Masoni, B. Minetti, P. Montagna, M. Morando, F. Nichitru, D. Panzieri, G. Pauli, M. Piccinini, G. Puddu, E. Rossetto, A. Rotondi, A. M. Rozhdestvensky, A. Saino, P. Salvini, L. Santi, M. G. Sapozhnikov, N. Semprini Cesari, S. Serici, R. Spighi, P. Temnikov, S. Tessaro, F. Tosello, V. Tretyak, G. L. Usai, S. Vecchi, L. Venturelli, M. Villa, A. Vitale, A. Zenoni, and A. Zoccoli, *Phys. Rev. Lett.* **74**, 371 (1995).
- ¹⁶R. Cabrera-Trujillo and B. D. Esry, *Radiat. Eff. Def. S.* **166**, 346 (2011).
- ¹⁷H. Tal Ezer and R. Kosloff, *J. Chem. Phys.* **81**, 3967 (1984).
- ¹⁸A. Nissen, H. O. Karlsson, and G. Kreiss, *J. Chem. Phys.* **133**, 054306 (2010).
- ¹⁹K. Andersson, F. Aquilante, A. Barysz, M. Bernhardsson, M. R. A. Blomberg, Y. Carissan, D. L. Cooper, M. Cossi, L. DeVico, N. Ferré, M. P. Fülscher, A. Gaenko, L. Gagliardi, G. Ghigo, C. de Graaf, S. Gusarov, B. A. Hess, D. Hagberg, A. Holt, G. Karlström, R. Lindh, P.-A. Malmqvist, T. Nakajima, P. Neogrády, J. Olsen, T. Pedersen, M. Pitonak, J. Raab, M. Reiher, B. O. Roos, U. Ryde, B. Schimmelpfennig, M. Schütz, L. Seijo, L. Serrano-Andrés, P. E. M. Siegbahn, J. Stårling, T. Thorsteinsson, V. Veryazov, and P.-O. Widmark, *J. Comp. Chem.* **31**, 224 (2014).
- ²⁰W. Domcke, D. R. Yarkony, and H. Köppel, *Conical Intersections*, Vol. 17 (WORLD SCIENTIFIC, 2011).
- ²¹W. Domcke and D. R. Yarkony, *Ann. Rev. Phys. Chem.* **63**, 325 (2012).
- ²²D. J. Tannor, *Introduction to Quantum Mechanics: A Time-Dependent Perspective* (University Science Books, 2006).
- ²³S. Zamith, C. Meier, N. Halberstadt, and J. A. Beswick, *J. Chem. Phys.* **110**, 960 (1999).
- ²⁴C. Cohen-Tannoudji, B. Diu, and F. Laloe, *Quantum Mechanics, Volume 1*, volume 1 ed. (Wiley-Interscience, 1977).
- ²⁵P. V. Demekhin and L. S. Cederbaum, *J. Chem. Phys.* **139**, 154314 (2013).
- ²⁶B. Desai, R., *Phys. Rev. Lett.* **119**, 1385 (1960).
- ²⁷K. K. Irikura, *J. Phys. Chem. Ref. Data* **36**, 389 (2007).
- ²⁸M. Kowalewski, J. Mikosch, R. Wester, and R. de Vivie-Riedle, *J. Phys. Chem. A* **118**, 4661 (2014).